Open Access

Journal of Energy and Power Technology

LIDSEN Publishing Inc.

Research Article

Variation of CO_2-Brine Contact Angles on Natural Rocks of Different Compositions

Foad Haeri [1, 2, *], Deepak Tapriyal [1, 2], Christopher Matranga [1], Dustin Crandall [1], Angela Goodman [1]

1. National Energy Technology Laboratory, 626 Cochrans Mill Road, P.O. Box 10940, Pittsburgh, PA 15236-0940, USA; E-Mails: mohammad.haeri@netl.doe.gov; deepak.tapriyal@netl.doe.gov; christopher.matranga@netl.doe.gov; dustin.crandall@netl.doe.gov; angela.goodman@netl.doe.gov
2. NETL Support Contractor, 626 Cochrans Mill Road, P.O. Box 10940, Pittsburgh, PA 15236-0940, USA

* **Correspondence:** Foad Haeri; E-Mail: mohammad.haeri@netl.doe.gov

Academic Editors: Nagasree Garapati and Megan Smith

Special Issue: Carbon Dioxide Utilization: Strategies for an Evolving Climate

Journal of Energy and Power Technology
2021, volume 3, issue 4
doi:10.21926/jept.2104046

Received: June 17, 2021
Accepted: October 25, 2021
Published: November 05, 2021

Abstract

Contact angles were measured for CO_2-brine interactions on 20 different rocks that represent the properties of various CO_2 storage depositional environments to characterize the wettability during geologic carbon storage. Three different CO_2 phases (gaseous, liquid, and supercritical) were considered to investigate the effect of pressure and temperature. Bubbles were studied in two groups of larger and smaller than 500 µm, the latter being more relevant to pore scale. Variation was observed among contact angle measurements, even while controlling the sample preparation and cleanliness. The contact angle variations could mainly be attributed to natural sample heterogeneity, as shown by an increased range of measured values for the smallest bubbles studied. Despite these variations, the analysis of 1139 contact angle measurements on 20 samples under 3 different experimental conditions showed that 92.8% of the angles were below 40°, meaning that the samples were primarily strongly-to-moderately water-wet with the average contact angle of 22°. 10% of the angles under

supercritical conditions were between 40° and 60°. This range of angles constitutes 5% and 4% of the measurements under liquid and gaseous conditions, respectively. Therefore, supercritical CO_2 was observed to be more wetting than liquid or gaseous CO_2.

Keywords

CO_2 storage; wettability; contact angle measurements; natural rocks; statistical analysis

1. Introduction

CO_2 storage as a well-known technique to reduce carbon footprint includes injection of CO_2 into depleted oil and gas reservoir or deep saline formations [1, 2]. Under the influence of buoyancy, the stored CO_2 tends to move upward in the formations but can be held trapped by different mechanisms, most importantly structural and residual trapping mechanisms [3].

Structural and residual trapping of CO_2 relies on capillary pressure [4] that depends on CO_2-brine interfacial tension (IFT), wettability behavior of the formation rock [5], and the pore structure of the rock, as shown in Eq. 1:

$$P_c = P_{CO_2} - P_{brine} = \frac{2\sigma \cos\theta}{r} \quad (1)$$

where P_c is the capillary pressure, P_{CO_2} is the pressure in the CO_2 phase, P_{brine} is the pressure in the brine phase, σ is the CO_2-brine IFT, r is the pore throat radius, and θ is the contact angle at the CO_2-brine-rock contact point (measured in the brine phase), representing the wettability of the rock. Some of intermediate-wet to CO_2-wet rocks that generate contact angles greater than 90°, makes the capillary pressure negative leading to the failure of structural trapping and significant reduction of residual trapping [3, 4, 6-9]. Brine as the typical wetting phase in the reservoirs can readily access all the pores, while CO_2 as the non-wetting phase gets trapped in the larger pores [10]. The wettability behavior of the formation rocks contacted by the invading CO_2 is impacted by multiple elements, such as rock type, surface heterogeneities, pressure, temperature, and brine salinity [3]. Wettability could also be influenced by the presence of organics [6-8], chemicals such as surfactant and nanoparticles [11], and CO_2-brine IFT [12, 13] in both sandstone and carbonate formations [14, 15].

Characterization of wettability through contact angle measurement has been the subject of multiple previous studies. Some focused on automatically measure the contact angle at in-situ conditions using micro computed tomography images [16-18]. Others studied interfacial energies between gas and liquid phases [19, 20], film thickness on the substrate [21], CO_2 phases during trapping [22, 23], wettability of cap rock minerals [24-26], and various acid gases [27]. The impact of pressure and temperature has also been investigated using common minerals, such as quartz and calcite [28, 29] and coal [30]. Other studies have focused on the effect of salt type, brine salinities, and surface charges [31-33] as well as surface contamination [34] and capillary pressure as a function of saturation [35, 36].

Despite many experimental attempts to characterize the wettability of formations, there seem to be discrepancies in the previous contact angle measurements. Other than differences in sample

preparation, CO_2-brine equilibration procedures, and experimental conditions, these discrepancies could mainly be attributed to natural sample heterogeneity generated by localized variations in topography, surface roughness, and mineral composition across the rock surface. Several parametric analyses correlated the variability of wettability behaviors to elements, such as rock type and compositions, CO_2 dissolution under different experimental conditions, surface contamination through preparing and cleaning the samples, and techniques to generate CO_2 bubbles and measure contact angles [37-39].

Some of these uncertainties were addressed in a recent work [40] by performing contact angle measurements on 6 different sandstone rocks. In this study, 14 other rocks of limestone, dolomite, shale, and other types are added to the investigation and the data on all the 20 rock samples are used to characterize the general wetting behavior of CO_2 under different experimental conditions. In a real subsurface system at these conditions, all the contact angles measured in this study could be present. Therefore, it is believed that the wettability behavior of the system will be best understood through a statistical analysis of the contact angles created by the bubbles.

2. Experimental Section

Rock samples were cut to size (1 in. × 0.5 in. × 0.126 in.) from the cores of 20 different reservoirs, including sandstones (Navajo, Nugget, Bentheimer, Bandera Brown, Berea, Mt. Simon and White Rim), limestones (Edward Brown and Edward Yellow), dolomite (Dolomite B and Dolomite S), shale (Bakken, Barnett, Eagle Ford and Mancos) and some other types, such as Carthage Marble (limestone), Austin Chalk, Lueders (carbonate reef), Limestone, and Basalt. The samples were not polished in order to observe the effects of differences in the surface roughness. The details of the sample preparation and cleaning along with other experimental procedure details are explained in our previous study [40] and also included in Appendix A. Synthetic brine was used as the solution for all the experiments, based on the Mt. Simon formation brine. Table 1 lists the composition of the brine.

Table 1 Mt. Simon synthetic brine composition [41].

Salt	g/L	Mw(g/mol)	mol/L
NaCl	61.67	58.443	1.0552
NaI	50.00	149.89	0.3336
$CaCl_2{\cdot}2H_2O$	78.35	147.02	0.5329
$MgCl_2{\cdot}6H_2O$	16.53	203.33	0.0813
KBr	6.480	119.00	0.0545
LiCl	9.364	42.394	0.2209
$SrCl_2{\cdot}6H_2O$	2.434	266.64	0.0091
Na_2SO_4	0.482	142.04	0.0034

The wettability behavior of 20 different rocks in contact with CO_2 and brine was analyzed using a customized contact angle measurement cell as illustrated in Figure 1. The measurements were performed using a captive method by generating CO_2 bubbles underneath the rock samples that were immersed in synthetic brine. Details of the setup are described in our previous work [40]. All lines and parts were cleaned with deionized water to remove any impurities, tested with high purity

nitrogen for leaks, and flushed with CO_2 to remove all air. The temperature of the system was maintained by an oven.

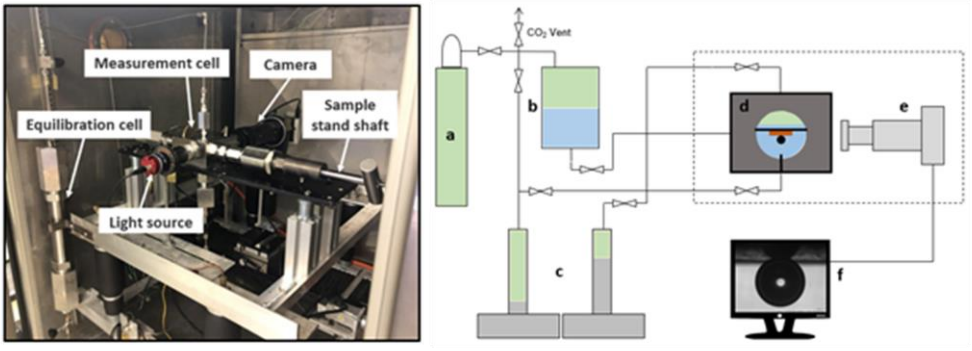

Figure 1 Contact angle measurement setup (left) and diagram (right): a-CO_2 cylinder, b-Equilibration cell, c-ISCO syringe pumps, d-Measurement cell, e-Light source, lenses and camera system, f-Image analysis.

First, the entire system was pressurized with CO_2 at 800 psig. After brine was equilibrated in the equilibration cell, CO_2 was added, and the CO_2-saturated brine was transferred to the measurement cell. To reach CO_2-brine phase equilibrium in the measurement cell, CO_2 was circulated between the equilibration cell and the measurement cell under gaseous (25°C & 800 psig) and supercritical conditions (45°C & 1800 psig). Once the CO_2 bubbles were generated, they were given time to stabilize in the system, so changes in the contact angles could only be associated with the wettability alteration rather than CO_2 dissolution. The contact angles were measured at the CO_2-rock-brine contact point within the aqueous side. Wettability behaviors were categorized relatively based on the contact angle ranges defined in Table 2.

Table 2 Contact angles and wettability behaviors [40].

Contact Angle (degrees)	Wettability Behavior
<20	Strongly Water-wet
20-40	Water-wet
40-60	Weakly Water-wet
60-120	Intermediate-wet
120-140	Weakly CO_2-wet
140-160	CO_2-wet
>160	Strongly CO_2-wet

3. Results and Discussions

In the previous work [40], mineralogical and surface characterization of six sandstone samples were performed using X-Ray Diffraction (XRD) and the surface heterogeneities were analyzed using Scanning Electron Microscope (SEM) images and optical profilometry. Additionally, surface elemental analysis was conducted using X-ray Photoelectron Spectroscopy (XPS) to verify the cleanliness of the samples throughout the experiments. The focus of this study is to analyze the contact angles on 20 different samples and characterize their wettability behavior.

Contact angles were measured at the contact point of static CO_2 bubbles (detached from the needle), brine, and the rock surface, when CO_2 was at equilibration with the synthetic brine under three experimental scenarios: 1-Gaseous CO_2 at 850 psig and 25°C (G-CO_2), 2-Liquid CO_2 at 1800 psig and 25°C (L-CO_2), and 3-Supercritical CO_2 at 1800 psig and 45°C (ScCO_2). Several bubbles with different diameters were generated and positioned at different spots on the rock surface. The variation of contact angles with bubble diameter for all 20 rock samples are depicted in Figures 2, 3, and 4 at G-CO_2, L-CO_2, and ScCO_2 conditions, respectively.

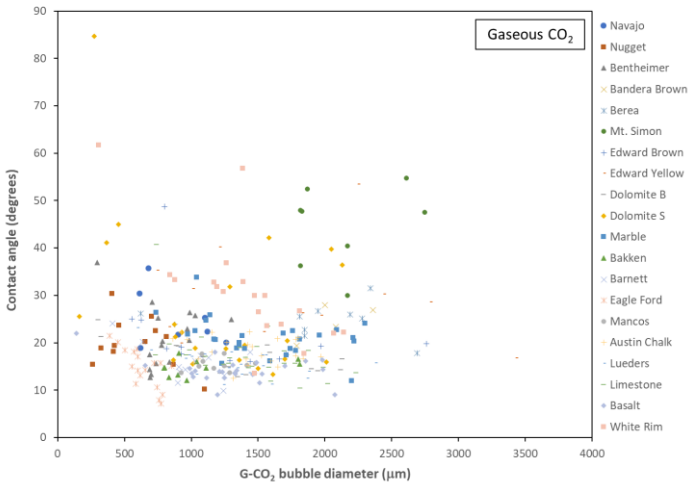

Figure 2 Contact angle versus CO_2 bubble diameter for 20 rock samples at gaseous CO_2 conditions (850 psig and 25°C).

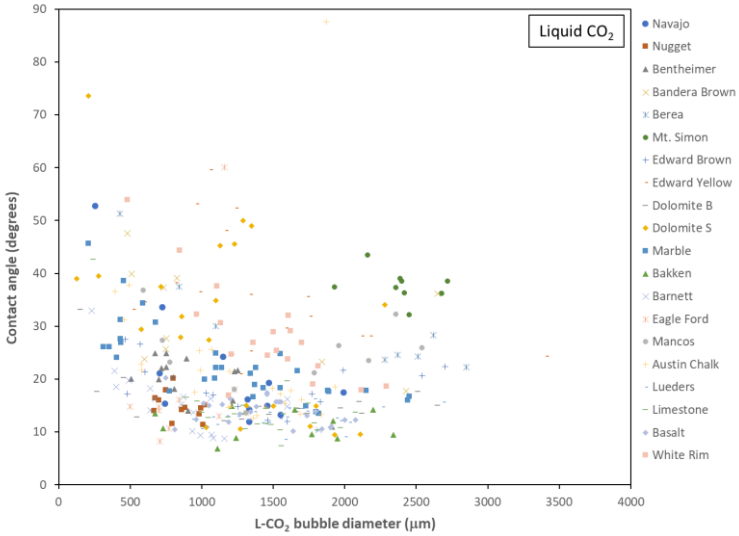

Figure 3 Contact angle versus CO_2 bubble diameter for 20 rock samples at liquid CO_2 conditions (1800 psig and 25°C).

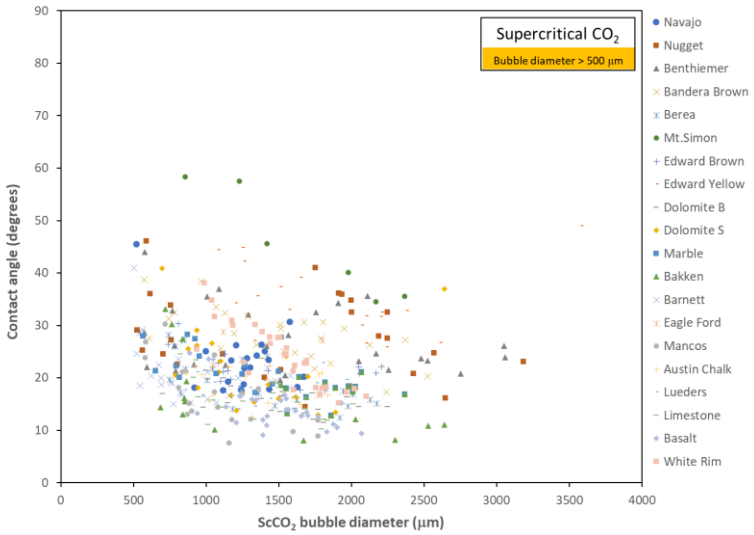

Figure 4 Contact angle versus CO_2 bubble diameter (> 500 µm) for 20 rock samples at supercritical conditions (1800 psig and 45°C).

Bubbles were essentially generated on a random base without controlling the size and position on the rock surface. The rock type, brine salinity, and environmental conditions (pressure and temperature) were fixed for each experiment. The influence of CO_2 dissolution into brine was eliminated by equilibrating the system using brine-saturated CO_2 bubbles in a CO_2-saturated brine environment. While the contact angles were largely populated between 10° and 40° at each experimental condition, no consistent trend was observed, which agrees with previous studies [23, 42-45]. Bubbles with a diameter smaller than 500 ⌈m generated at supercritical conditions are of interest for future studies because they are most representative of the behavior in pores at deep saline storage conditions. The contact angles associated with these bubbles revealed a higher level of variation (15°-80°) as plotted in Figure 5. These variations are likely related to the impact of surface asperities and roughness, which were qualitatively studied before [40] by SEM imaging and profilometry analysis.

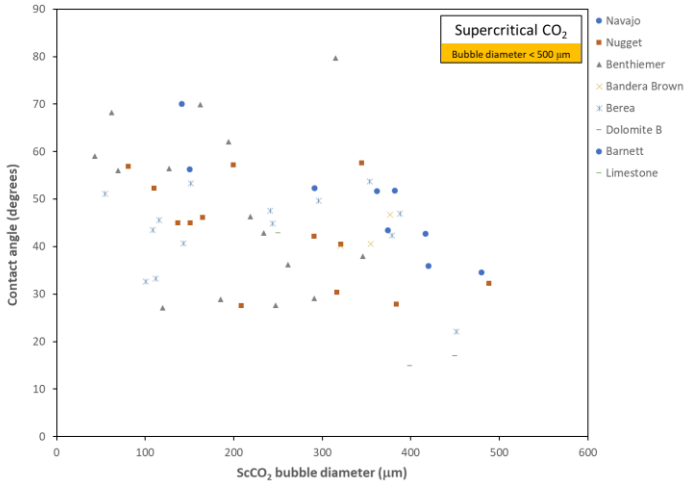

Figure 5 Contact angle versus CO_2 bubble diameter (< 500 µm) for some samples at supercritical conditions (1800 psig and 45°C).

Variability in contact angles due to highly localized surface heterogeneity was observed across all the experiments in this study with different rock samples and various CO_2 bubble diameters. The impact of surface roughness on variability of contact angles has been recognized for decades [46-50] and addressed in our previous work [40] as well. In this study, a large number of contact angle measurements and samples are used to discern some general trends on the wettability behavior.

As seen in Figure 6, the histograms of all the measured contact angles across three different experimental conditions (1139 measurements for 20 samples) are skewed to the right and mainly concentrated between 10° and 25°. The normal distribution shows that most of the angles (about 92.8%) represent strongly to moderately water-wet behavior (angles smaller than 40°) based on the categories defined in Table 2. Only a slight portion of the measurements (about 7.8%) relate to weakly water-wet behavior (angles larger than 40°) as depicted in the distribution. The angles range between 7° and 88° with a mean of 22° and standard deviation of 11°. The mode and median are 17° and 19° respectively.

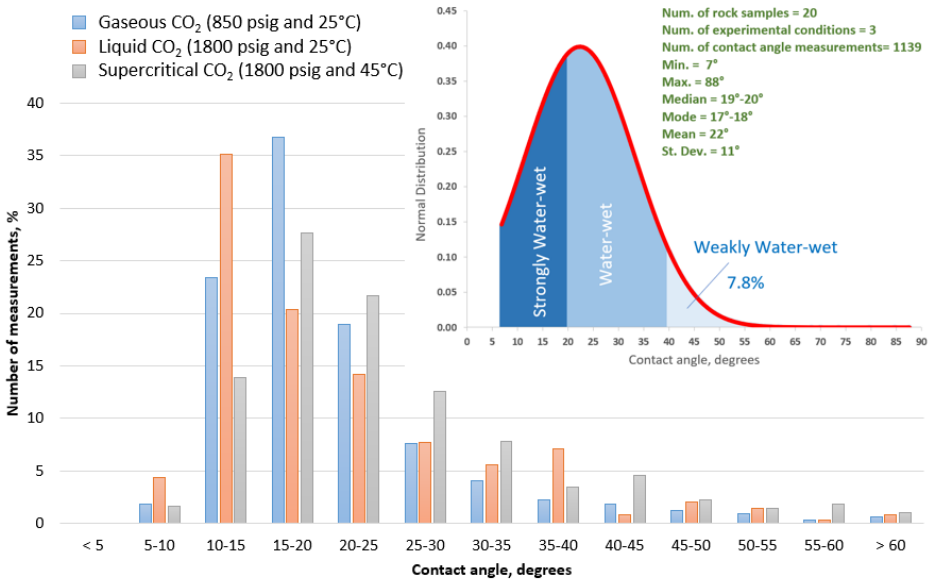

Figure 6 Histograms of contact angles across different experimental conditions.

The diagram in Figure 7 also shows that a major portion of the contact angles belongs to strongly water-wet (green zone) and moderately water-wet (blue zone) behavior, that is 95%, 94%, and 89% under gaseous, liquid, and supercritical conditions respectively. Additionally, the share of weakly water-wet (yellow zone) is largest under supercritical conditions (10%) compared to liquid (5%) and gaseous (4%), meaning the rock samples show more weakly water-wet behavior with $ScCO_2$ that with L-CO_2 or G-CO_2. In other words, supercritical CO_2 seems to be more wetting than liquid or gas CO_2. Only 1% of the angles represent a wettability behavior that could not be described as water-wet ($q > 60°$).

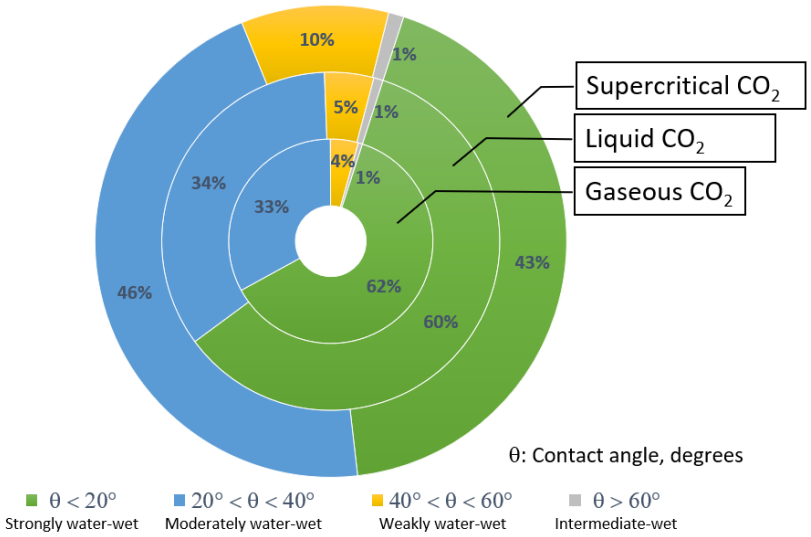

Figure 7 Contact angle distributions and wettability characterization.

The variations in the contact angles of this and previous [40] studies demonstrate that the physical and chemical characteristics of the rock samples in interaction with CO_2 and brine are very complex and the parameters involved in the process of equilibration and measurements are poorly understood making the wettability characterization challenging. Despite these challenges, the results of this study revealed that it is still possible to characterize wettability by controlling experimental conditions, conducting comprehensive physical and chemical characterization of the natural samples, and statistically analyzing several bubbles of varying size on different rock samples at different experimental conditions.

4. Conclusions

The variation of CO_2-brine contact angles was investigated in this study using 20 natural rock samples of different formations. Our previous study on sandstone rocks showed that, despite of carefully controlling the sample preparation, equilibration process, and CO_2 phase behavior, it was difficult to find any correlation between contact angles and other variables, such as surface roughness, grain sizes, or chemical heterogeneity caused by different minerals in these grains. However, this study showed that it is possible to statistically analyze the contact angle measurements to characterize a general wetting behavior of CO_2 on different rocks. By analyzing 1139 bubbles on all 20 samples across three phases of CO_2, it was found that most of the angles are concentrated between 15° and 25° and about 92.8% of the contact angles were below 40°, classified as strongly water-wet to moderately water-wet. Since all the contact angles measured in this study could exist in a real subsurface system at the conditions tested, it is believed that the wettability behavior of the system will be best understood through a statistical analysis of the contact angles created by the bubbles.

Appendix A:

Details of Experimental Procedure [40]

Sample Preparation

All samples were cleaned for 5 min. using a Harrick Plasma Cleaner (model PDC-32G) at medium Radio Frequency (RF) level with air as a carrier gas. X-ray Photoelectron Spectroscopy (XPS) data were collected after cutting (before cleaning), after cleaning, and after contact angle measurements to identify possible effects from surface contamination and also to note any effect that the exposure to brine and CO_2 may have on the surface during those measurements. XPS analysis was carried out with a ULVAC-PHI Versa Probe III instrument using a focused (100 µm) monochromatized Al Kα X-ray source (1486.6 eV). The pass energy of the analyzer was 55.5 eV for high-resolution scans. Binding energies were calibrated using the C 1s peak for adventitious carbon, which was assigned a binding energy of 284.8 eV. Elemental atomic concentrations were calculated from high-resolution spectra using PHI-provided sensitivity factors.

Experimental Setup

The wettability behavior of 20 different rock samples in contact with CO_2 and brine was evaluated using a customized contact angle measurement cell. The contact angle measurements were performed using captive bubble method by generating $ScCO_2$ bubbles underneath the rock samples immersed in synthetic brine. The high-pressure Hastelloy® measurement cell was custom designed for pressures up to 10,000 psig and temperatures up to 150 °C. The cell has two high-pressure sapphire windows (0.5 in.) to facilitate imaging and lighting. Window holders are designed to be O-ring free to avoid any contamination from the O-ring or sealing material. The cell uses metal-to-metal (coned and thread) sealing commonly used for high-pressure fittings. The rock samples were mounted inside the high-pressure cell on a Hastelloy® stand, which is connected to a shaft. The shaft can be rotated 360° and moved horizontally up to 3 inches. Multiple samples can be mounted on the sample stand as desired. A separate high-pressure cell serves as equilibration cell. Both measurement and the equilibration cell are partially filled with brine. In the measurement cell samples are completely immersed in brine. Then CO_2 is added to reach desired pressure. After that CO_2 is circulated in the system from measurement cell to equilibration cell and then back to measurement cell using pair of pumps. Finally, CO_2 and brine are equilibrated overnight under desired temperature and pressure prior to conducting contact angle measurements. After the experiment, pumps are used to decrease the pressure of the cells to the CO_2 tank pressure and then needle valves are opened very slowly to vent the rest of CO_2. Fluid movement in the system was achieved by using two Teledyne 260D ISCO® syringe pumps controlled in LabVIEW®. The pumps are used to bring CO_2 to high pressures, generate CO_2 bubbles, equilibrate CO_2 and brine, and maintain pressure during the measurements. All the tubing, valves, and fittings are made of 316 stainless steel. Lighting was provided by a Telocentric HP blue illuminator and visualization by a Leica NC 170HD camera with Z16 APO zoom system. The DropSnake plugin for ImageJ[48] was used to analyze the captured images for contact angle evaluation. Figure 3 illustrates the schematic diagram of the entire experimental setup.

Contact Angle Measurement Procedure

Before each experiment, all lines and cell parts of the contact angle measurement systems were cleaned with deionized water to remove any impurities. High purity nitrogen was used to test the set-up for leaks and CO_2 was used to flush the system to remove all air. The temperature of the contact angle measurement system was maintained by an oven. Initially, the entire system was pressurized with CO_2 at CO_2 tank pressure (800 psig). Once brine was equilibrated in the equilibration cell, CO_2 was added using one of the pumps and CO_2-saturated brine was transferred to the measurement cell. CO_2 was circulated between the equilibration cell and the measurement cell until the phase equilibration between CO_2 and brine was reached in the measurement cell. The circulation process to equilibrate the system was conducted for two different experimental conditions (25°C & 800 psig and 45°C & 1800 psig) representing CO_2 at both gaseous and supercritical conditions, respectively. For high pressures and supercritical experiments, the experimental conditions need to be reached before the equilibration process can start. A small head of CO_2 was left above the brine in the measurement cell to facilitate the equilibration. Once the equilibration was completed, CO_2 bubbles were generated and observed for at least 1 h to ensure there were no changes in the bubble diameter due to dissolution of CO_2 into brine. Therefore, any variation of contact angles could only be related to the wettability alteration of the rock sample rather than dissolution of CO_2 into the solution. After confirming the stability of the bubble diameter, the bubble images were captured by the camera and the contact angles were measured at the interface of the CO_2 bubble, rock sample, and brine. In order to observe the actual contact point of the bubble with the rock surface and correctly measure the contact angle, the camera was slightly tilted with respect to the horizontal line and proper magnification and lighting exposure settings were selected before capturing the image. Several bubbles were captured and analyzed at each experimental condition to confirm the repeatability of the measurements. The angles were measured in the aqueous side (brine) as the denser phase.

Acknowledgment

This work was performed in support of the U.S. Department of Energy's Fossil Energy Crosscutting Technology Research Program. The research was executed through the NETL Research and Innovation Center's Carbon Storage Field Work Proposal. This research was supported in part by an appointment to the National Energy Technology Laboratory Research Participation Program, sponsored by the U.S. Department of Energy.

Author Contributions

Foad Haeri: Methodology, Data Acquisition, Analysis, Visualization, Writing-Original Draft. Deepak Tapriyal: Methodology, Data Acquisition, Analysis, Writing-Review & Editing. Christopher Matranga: Validation, Analysis, Writing-Review & Editing. Dustin Crandall: Sample Acquisition, Validation, Writing-Review & Editing. Angela Goodman: Supervision, Validation, Writing-Review & Editing.

Funding

This work was funded by the Department of Energy, National Energy Technology Laboratory, an agency of the United States Government, through a support contract with Leidos Research Support Team (LRST).

Competing Interests

Neither the United States Government nor any agency thereof, nor any of their employees, nor LRST, nor any of their employees, makes any warranty, expressed or implied, or assumes any legal liability or responsibility for the accuracy, completeness, or usefulness of any information, apparatus, product, or process disclosed, or represents that its use would not infringe privately owned rights. Reference herein to any specific commercial product, process, or service by trade name, trademark, manufacturer, or otherwise, does not necessarily constitute or imply its endorsement, recommendation, or favoring by the United States Government or any agency thereof. The views and opinions of authors expressed herein do not necessarily state or reflect those of the United States Government or any agency thereof.

References

1. Metz B, Davidson O, de Coninck H, Loos M, Meyer L. Carbon dioxide capture and storage. New York: Cambridge University Press; 2005.
2. Thomas DC. Carbon dioxide capture for storage in deep geologic formations-results from the CO_2 capture project. In: Geologic storage of carbon dioxide with monitoring and verification. Amsterdam, Netherlands: Elsevier; 2015.
3. Iglauer S. CO_2-water-rock wettability: Variability, influencing factors, and implications for CO_2 geostorage. Acc Chem Res. 2017; 50: 1134-1142.
4. Arif M, Al-Yaseri A, Barifcani A, Lebedev M, Iglauer S. Impact of pressure and temperature on CO_2-brine-mica contact angles and CO_2-brine interfacial tension: Implications for carbon geo-sequestration. J Colloid Interface Sci. 2016; 462: 208-215.
5. Chalbaud C, Robin M, Lombard JM, Martin F, Egermann P, Bertin H. Interfacial tension measurements and wettability evaluation for geological CO_2 storage. Adv Water Resour. 2009; 32: 98-109.
6. Ali M, Sahito MF, Jha NK, Arain Z, Memon S, Keshavarz A, et al. Effect of nanofluid on CO_2-wettability reversal of sandstone formation; implications for CO_2 geo-storage. J Colloid Interface Sci. 2020; 559: 304-312.
7. Ali M, Arif M, Sahito MF, Al-Anssari S, Keshavarz A, Barifcani A, et al. CO_2-wettability of sandstones exposed to traces of organic acids: Implications for CO_2 geo-storage. Int J Greenh Gas Control. 2019; 83: 61-68.
8. Ali M, Al-Anssari S, Arif M, Barifcani A, Sarmadivaleh M, Stalker L, et al. Organic acid concentration thresholds for ageing of carbonate minerals: Implications for CO_2 trapping/storage. J Colloid Interface Sci. 2019; 534: 88-94.
9. Spiteri EJ, Juanes R, Blunt MJ, Orr FM. A new model of trapping and relative permeability hysteresis for all wettability characteristics. SPE J. 2008; 13: 277-288.

10. Juanes R, Spiteri EJ, Orr FM, Blunt MJ. Impact of relative permeability hysteresis on geological CO_2 storage. Water Resour Res. 2006; 42: W12418.
11. Jha NK, Ali M, Iglauer S, Lebedev M, Roshan H, Barifcani A, et al. Wettability alteration of quartz surface by low-salinity surfactant nanofluids at high-pressure and high-temperature conditions. Energy Fuels. 2019; 33: 7062-7068.
12. Jha NK, Ali M, Sarmadivaleh M, Iglauer S, Barifcani A, Lebedev M, et al. Low salinity surfactant nanofluids for enhanced CO_2 storage application at high pressure and temperature. Proceedings of the fifth CO_2 geological storage workshop; 2018 November 21-23; Utrecht, Netherlands.
13. Al-Anssari S, Arain ZU, Barifcani A, Keshavarz A, Ali M, Iglauer S. Influence of pressure and temperature on CO_2-nanofluid interfacial tension: Implication for enhanced oil recovery and carbon geosequestration. Proceedings of the Abu Dhabi International Petroleum Exhibition & Conference; 2018 November 12-15; Abu Dhabi, UAE.
14. Arain ZU, Al-Anssari S, Ali M, Memon S, Bhatti MA, Lagat C, et al. Reversible and irreversible adsorption of bare and hybrid silica nanoparticles onto carbonate surface at reservoir condition. Petroleum. 2020; 6: 277-285.
15. Ali M, Al-Anssari S, Shakeel M, Arif M, Dahraj NU, Iglauer S. Influence of miscible CO_2 flooding on wettability and asphaltene precipitation in Indiana limestone. Proceedings of the SPE/IATMI Asia Pacific Oil & Gas Conference and Exhibition; 2017 October 17-19: Jakarta, Indonesia.
16. Scanziani A, Singh K, Blunt MJ, Guadagnini A. Automatic method for estimation of in situ effective contact angle from X-ray micro tomography images of two-phase flow in porous media. J Colloid Interface Sci. 2017; 496: 51-59.
17. AlRatrout A, Raeini A, Bijeljic B, Blunt MJ. Automatic measurement of contact angle in pore-space images. Adv Water Resour. 2017; 109: 158-169.
18. Yang J, Zhou Y. An automatic in-situ contact angle determination based on level set method. Water Resour Res. 2020; 56: e2020WR027107.
19. Dickson JL, Gupta G, Horozov TS, Binks BP, Johnston KP. Wetting phenomena at the CO_2/water/glass interface. Langmuir. 2006; 22: 2161-2170.
20. Zheng X, Barrios AC, Perreault F, Yun TS, Jang J. Interfacial tension and contact angle in CO_2-water/nanofluid-quartz system. Greenh Gas Sci Technol. 2018; 8: 734-746.
21. Li Y, Pham JQ, Johnston KP, Green PF. Contact angle of water on polystyrene thin films: Effect of CO_2 environment and film thickness. Langmuir. 2007; 23: 9785-9793.
22. Sutjiadi-Sia Y, Jaeger P, Eggers R. Interfacial phenomena of aqueous systems in dense carbon dioxide. J Supercrit Fluids. 2008; 46: 272-279.
23. Mutailipu M, Liu Y, Jiang L, Zhang Y. Measurement and estimation of CO_2-brine interfacial tension and rock wettability under CO_2 sub- and super-critical conditions. J Colloid Interface Sci. 2019; 534: 605-617.
24. Wang S, Edwards IM, Clarens AF. Wettability phenomena at the CO_2-brine-mineral interface: Implications for geologic carbon sequestration. Environ Sci Technol. 2013; 47: 234-241.
25. Chiquet P, Broseta D, Thibeau S. Wettability alteration of caprock minerals by carbon dioxide. Geofluids. 2007; 7: 112-122.
26. Tonnet N, Broseta D. Evaluation of the petrophysical properties of a carbonate-rich caprock for CO_2 geological storage purposes. Proceedings of the SPE EUROPEC/EAGE Annual Conference and Exhibition; 2010 June 14-17; Barcelona, Spain.

27. Shah V, Broseta D, Mouronval G. Capillary alteration of caprocks by acid gases. Proceedings of the SPE/DOE Improved Oil Recovery Symposium; 2009 April 19-23; Tulsa, Oklahoma, USA.
28. Bikkina PK. Contact angle measurements of CO_2-water-quartz/calcite systems in the perspective of carbon sequestration. Int J Greenh Gas Control. 2011; 5: 1259-1271.
29. Sarmadivaleh N, Al-Yaseri AZ, Iglauer S. Influence of temperature and pressure on quartz-water-CO_2 contact angle and CO_2-water interfacial tension. J Colloid Interface Sci. 2015; 441: 59-64.
30. Siemons N, Briuning H, Castelijns H, Wolf K. Pressure dependence of the contact angle in a CO_2-H_2O-coal system. J Colloid Interface Sci. 2006; 297: 755-761.
31. Al-Yaseri AZ, Lebedev M, Barifcani A, Iglauer S. Receding and advancing (CO_2-brine-quartz) contact angles as a function of pressure, temperature, surface roughness, salt type, and salinity. J Chem Thermodyn. 2021; 196: 107673.
32. Chen Y, Sari A, Xie Q, Brady PV, Hossain MM, Saeedi A. Electrostatic origins of CO_2-increased hydrophilicity in carbonate reservoirs. Sci Rep. 2018; 8: 1-9.
33. Chen Y, Sari A, Xie Q, Saeedi A. Insights into wettability alteration of CO_2-assisted EOR in carbonate reservoirs. J Mol Liq. 2019; 279: 420-426.
34. Mahadevan J. Comments on the paper titled "Contact angle measurements of CO_2-water-quarts/calcite systems in the perspective of carbon sequestration": A case of contamination? Int J Greenh Gas Control. 2012; 7: 261-262.
35. Plug WJ, Bruining J. Capillary pressure for sand-CO_2-water under various pressure conditions. application to CO_2 sequestration. Adv Water Resour. 2007; 30: 2339-2353.
36. Jafari M, Jung J. Variation of contact angles in brine/CO_2/mica system considering short-term geological CO_2 sequestration condition. Geofluids. 2018; 2018: 1-15.
37. Garing C, Benson SM. CO_2 wettability of sandstones: Addressing conflicting capillary behaviors. Geophys Res Lett. 2018; 46: 776-782.
38. Arif M, Abu-Khamsin SA, Iglauer S. Wettability of rock/CO_2/brine and rock/oil/CO_2-enriched-brine systems: Critical parametric analysis and future outlook. Adv Coll Interface Sci. 2019; 268: 91-113.
39. Wan J, Kim Y, Tokunaga TK. Contact angle measurement ambiguity in supercritical CO_2-water-mineral systems: Mica as an example. Int J Greenh Gas Control. 2014; 31: 128–137.
40. Haeri F, Tapriyal D, Sanguinito S, Shi F, Fuchs SJ, Dalton LE, et al. CO_2–brine contact angle measurements on Navajo, Nugget, Bentheimer, Bandera Brown, Berea, and Mt. Simon Sandstones. Energy Fuels. 2020; 34: 6085-6100.
41. Dalton LE, Klise K, Fuchs S, Crandall D, Goodman A. Methods to measure contact angles in $ScCO_2$-brine-sandsone systems. Adv Water Resour. 2018; 122: 278-290.
42. Farokhpoor R, Bjørkvik BJ, Lindeberg E, Torsæter O. CO_2 wettability behavior during CO_2 sequestration in saline aquifer-an experimental study on minerals representing sandstone and carbonate. Energy Procedia. 2013; 37: 5339-5351.
43. Botto J, Fuchs SJ, Fouke BW, Clarens AF, Freiburg JT, Berger PM, et al. Effects of mineral surface properties on supercritical CO_2 wettability in a siliciclastic reservoir. Energy Fuels. 2017; 31: 5275-5285.
44. Shojai Kaveh N, Rudolph ES, van Hemert P, Rossen WR, Wolf KH. Wettability evaluation of a CO_2/water/bentheimer sandstone system: Contact angle, dissolution, and bubble size. Energy Fuels. 2014; 28: 4002-4020.

45. Alnili F, Al-Yaseri A, Roshan H, Rahman T, Verall M, Lebedev M, et al. Carbon dioxide/brine wettability of porous sandstone versus solid quartz: An experimental and theoretical investigation. J Colloid Interface Sci. 2018; 524: 188-194.
46. Morrow NR. The effects of surface roughness on contact angle with special reference to petroleum recovery. J Can Pet Technol. 1975; 14. doi:10.2118/75-04-04.
47. Lin FY, Li D, Neumann AW. Effect of surface roughness on the dependence of contact angles on drop size. J Colloid Interface Sci. 1993; 159: 86-95.
48. Drelich J, Miller J, Good R. The effect of drop (bubble) size on advancing and receding contact angles for heterogeneous and rough solid surfaces as observed with sessile-drop and captive-bubble techniques. J Colloid Interface Sci. 1996; 179: 37-50.
49. Tadmor R. Line energy, line tension and drop size. Surf Sci. 2008; 602: L108-L111.
50. Duursma GR, Sefiane K, David S. Advancing and receding contact lines on patterned structured surfaces. Chem Eng Res Design. 2009; 88: 737-743.